IEEE Access
Multidisciplinary | Rapid Review | Open Access Journal

Received September 22, 2016, accepted September 27, 2016, date of publication December 8, 2016, date of current version January 27, 2017.

Digital Object Identifier 10.1109/ACCESS.2016.2636166

Orbital Angular Momentum (OAM) Generation by Cylinder Dielectric Resonator Antenna for Future Wireless Communications

JIAJUN LIANG, (Student Member, IEEE), AND SHENGLI ZHANG, (Member, IEEE)
School of Information Engineering, Shenzhen University, Shenzhen 518060, China

Corresponding author: S. Zhang (zsl@szu.edu.cn)

This work was supported in part by the National Natural Science Foundation of China under Grant 61372078 and in part by the Natural Science Foundation of Guangdong under Grant 2014A030313549.

ABSTRACT In this paper, we demonstrate that the solid cylinder dielectric resonator antenna (CDRA) is a high radiation efficient device to generate orbital angular momentum (OAM) waves with different OAM modes at different frequencies. Theoretical formulations of its radiation fields are deduced in the cylindrical coordinate system, which shows that all components of the electric and magnetic fields have the azimuth dependence of $e^{jm\varphi}$. A full-wave simulation on a practical size CDRA is then implemented to validate the theoretical derivations. The simulation results show that different separated OAM modes can be obtained at different frequencies. Specifically, the higher order OAM modes are generated at higher electron magnetic modes, which makes CDRA a promising method to overcome the narrow band and multiband issues existing in the design of current OAM devices. Furthermore, a maximum radiation efficiency of 97.1% at 13.3 GHz, and a minimum radiation efficiency of 72.4% at 19.45 GHz are obtained in our simulation, which is a high radiation efficiency feature at the OAM resonant frequencies.

INDEX TERMS Cylinder dielectric resonator antenna, orbital angular momentum, high radiation efficient.

I. INTRODUCTION

Orbital angular momentum (OAM) has grown into a large research field with numerous applications in the domains of terahertz communication [1], video transmission [2], biomedical engineerings [3], and imaging [4]. Research indicates that OAM allows the possibility of transmitting multiple signals simultaneously at the same frequency with different OAM modes. This can be used to increase the channel multiplexing and potentially improve the spectrum efficiency [5]. OAM based radio frequency communication has become a hot research field after the first laboratory experiment of OAM radio beam generation was presented in [6]. In order to satisfy the needs of diverse applications, there are many schemes for the generation of OAM radio beams, such as the single patch antenna [7], spiral phase plate [8], phased array [9], metamaterial antenna [10], and horn lens antenna [11].

A dielectric resonator (DR), which is a kind of low loss material with high relative permittivity, has become a novel electromagnetic device for antenna design. The antenna system which applies a DR as the radiator is called dielectric resonator antenna (DRA). DRA offers many outstanding features. The first is size reduction - the dimension of a DRA is in the order of $\frac{\lambda_0}{\sqrt{\varepsilon_r}}$, where λ_0 is the free space wavelength and ε_r is the dielectric constant of the DR material. By choosing a high value of ε_r, the size of the DRA can be significantly reduced with no inherent conductor loss in dielectric resonators. The second is high radiation efficiency. The third is the multiple modes radiator – the operating band of a DRA can be varied over a wide range by suitably choosing DR parameters. These excellent properties of the DRA in terms of low loss, low profile and high radiation efficiency makes it an attractive method for OAM antenna design.

Much research has been done on the transmission characteristics of DRA [11]–[16]. To our best knowledge, the only paper exhibiting an OAM beam generated by DRA was [17], where the authors provides a simple analysis, a numerical simulation and an experiment to demonstrate the OAM features. To obtain the theoretical analysis, the intuitive model, replacing the ring with equivalent circular dipoles, is adopted in [17]. Without this equivalence assumption, we directly derive the EM wave expressions based on Maxwell

equations for the DRA, satisfying certain boundary conditions. In particular, this paper provides a detailed theoretical explanation of OAM waves propagating along a solid cylindrical dielectric resonator antenna (CDRA).

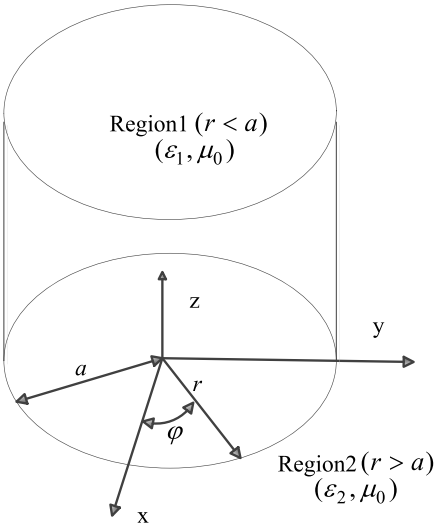

FIGURE 1. CDRA immersed in an infinite medium.

II. THEORETICAL MODEL AND ANALYSIS

In order to study the transmission characteristics inside or outside the DRA, we need to first calculate the electromagnetic field distribution of a solid cylinder dielectric resonator antenna (CDRA) in a cylindrical coordinate system. The theoretical model of the CDRA is shown in Fig.1. A CDRA of radius a divides the space into two regions: *Region* 1 denoting the space inside the CDRA ($r < a$) and *Region* 2 denoting the opening air space outside the CDRA ($r > a$).[1] The permittivity in *Region* 1 is ε_1 and the permittivity in *Region* 2 is ε_2, where we assume that $\varepsilon_1 > \varepsilon_2$. In both regions, the permeability is the same μ_0.

Without loss of generality, our analysis is based on two basic principles: guided waves are governed by the source-free Maxwell equations [12] and the total electromagnetic field can be separated into partial fields. The guided wave modes propagate along a perfectly straight line path, and every component of the electromagnetic wave can be represented in the form $f(u, v)e^{-j\beta z+j\omega t}$, where z is chosen as the propagation direction, u and v are the generalized orthogonal coordinates in the transverse plane. In the following, the factor $e^{-j\beta z+j\omega t}$ will be suppressed for simplicity. Then, the scalar Helmoholtz equation in the cylindrical coordinate system(r, φ, z) can be written as

$$\frac{\partial^2 E_z}{\partial r^2} + \frac{1}{r}\frac{\partial E_z}{\partial r} + \frac{1}{r^2}\frac{\partial^2 E_z}{\partial \varphi^2} + k_c^2 E_z = 0 \tag{1}$$

$$\frac{\partial^2 H_z}{\partial r^2} + \frac{1}{r}\frac{\partial H_z}{\partial r} + \frac{1}{r^2}\frac{\partial^2 H_z}{\partial \varphi^2} + k_c^2 H_z = 0 \tag{2}$$

[1]The length of the CDRA is assumed to be infinite.

and every component of the electromagnetic field can be obtained as

$$E_r = \frac{1}{k_c^2}(-j\beta\frac{\partial E_z}{\partial r} - \frac{j\omega\mu}{r}\frac{\partial H_z}{\partial \varphi}) \tag{3}$$

$$E_\varphi = \frac{1}{k_c^2}(-\frac{j\beta}{r}\frac{\partial E_z}{\partial \varphi} + j\omega\mu\frac{\partial H_z}{\partial r}) \tag{4}$$

$$H_r = \frac{1}{k_c^2}(\frac{j\omega\varepsilon}{r}\frac{\partial E_z}{\partial \varphi} - j\beta\frac{\partial H_z}{\partial r}) \tag{5}$$

$$H_\varphi = \frac{1}{k_c^2}(-j\omega\varepsilon\frac{\partial E_z}{\partial r} - \frac{j\beta}{r}\frac{\partial H_z}{\partial \varphi}) \tag{6}$$

with $k_c^2 = \omega^2\mu\varepsilon - \beta^2$ (β is the propagation constant).

In *Region* 1, the equations (1) and (2) can be solved by using separation of variables [12], [13]. Let $k_c^2 = k_{c1}^2$, k_{c1} is the cutoff wavenumber in *Region* 1. The electric and magnetic field expressions can be derived from (1)–(2) as follows:

$$E_z^1(r, \varphi) = \sum_{m=0}^{\infty}\sum_{n=1}^{\infty} A_{mn}J_m(k_{c1}r)e^{jm\varphi} \tag{7}$$

$$H_z^1(r, \varphi) = \sum_{m=0}^{\infty}\sum_{n=1}^{\infty} B_{mn}J_m(k_{c1}r)e^{jm\varphi} \tag{8}$$

$$k_{c1}^2 = \omega^2\mu_0\varepsilon_1 - \beta^2 \tag{9}$$

where the coefficients A_{mn} and B_{mn} are decided by matching the boundary conditions. Here m can be any integer greater than or equal to zero, n can be arbitrary integer greater than zero, β is the propagation constant. $J_m(k_{c1}r)$ is the Bessel function of the first kind of order m with $k_{c1}r$ as the argument. For an actual size CDRA with radius a, we can calculate the cutoff wavenumber $k_{c1mn} = \frac{u_{mn}}{a}$, where u_{mn} is the nth root of $J_m(k_{c1}r)$. The transverse fields can be obtained by substituting the expressions (7)–(8) into the equaions (3)–(6). Thus, we have

$$E_r^1(r, \varphi) = \frac{1}{k_{c1}^2}\sum_{m=0}^{\infty}\sum_{n=1}^{\infty}[-j\beta k_{c1}A_{mn}J_m'(k_{c1}r) + \frac{\omega\mu_0 m}{r}B_{mn}J_m(k_{c1}r)]e^{jm\varphi} \tag{10}$$

$$E_\varphi^1(r, \varphi) = \frac{1}{k_{c1}^2}\sum_{m=0}^{\infty}\sum_{n=1}^{\infty}[\frac{\beta m}{r}A_{mn}J_m(k_{c1}r) + j\omega\mu_0 k_{c1}B_{mn}J_m'(k_{c1}r)]e^{jm\varphi} \tag{11}$$

$$H_r^1(r, \varphi) = \frac{1}{k_{c1}^2}\sum_{m=0}^{\infty}\sum_{n=1}^{\infty}[\frac{-\omega\varepsilon_1 m}{r}A_{mn}J_m(k_{c1}r) - j\beta k_{c1}B_{mn}J_m'(k_{c1}r)]e^{jm\varphi} \tag{12}$$

$$H_\varphi^1(r, \varphi) = \frac{1}{k_{c1}^2}\sum_{m=0}^{\infty}\sum_{n=1}^{\infty}[-j\omega\varepsilon_1 k_{c1}A_{mn}J_m'(k_{c1}r) + \frac{\beta l}{r}B_{mn}J_m(k_{c1}r)]e^{jm\varphi} \tag{13}$$

The prime, $J_m'(k_{c1}r)$ signifies the derivative of the function with respect to its argument $k_{c1}r$.

In *Region* 2, all field components will decay to zero as $r \to \infty$. Then we let $k_c^2 = -k_{c2}^2$, k_{c2} is the cutoff wavenumber in *Region* 2. The electric and magnetic field expressions can be derived from (1)–(2) as follows:

$$E_z^2(r,\varphi) = \sum_{m=0}^{\infty}\sum_{n=1}^{\infty} C_{mn}K_m(k_{c2}r)e^{jm\varphi} \tag{14}$$

$$H_z^2(r,\varphi) = \sum_{m=0}^{\infty}\sum_{n=1}^{\infty} D_{mn}K_m(k_{c2}r)e^{jm\varphi} \tag{15}$$

where $K_m(k_{c2}r)$ is the modified Bessel function of the second kind of order m and $k_{c2}r$ is the argument. Here, the modified Bessel function $K_m(k_{c2}r)$ is chosen since as $r \to \infty$, $K_m(k_{c2}r) \to 0$, as required by the radiation condition at ∞. The coefficients C_{mn} and D_{mn} are decided by matching the boundary conditions. Here m can be any integer greater than or equal to zero, n can be any arbitrary integer greater than zero. β is the propagation constant, and

$$k_{c2}^2 = \beta^2 - \omega^2\mu_0\varepsilon_2 \tag{16}$$

The transverse fields can be obtained by substituting expressions (14)–(15) into (3)–(6). We have

$$E_r^2(r,\varphi) = -\frac{1}{k_{c2}^2}\sum_{m=0}^{\infty}\sum_{n=1}^{\infty}[-j\beta k_{c2}C_{mn}K_m'(k_{c2}r) + \frac{\omega\mu_0 m}{r}D_{mn}K_m(k_{c2}r)]e^{jm\varphi} \tag{17}$$

$$E_\varphi^2(r,\varphi) = -\frac{1}{k_{c2}^2}\sum_{m=0}^{\infty}\sum_{n=1}^{\infty}[\frac{\beta m}{r}C_{mn}K_m(k_{c2}r) + j\omega\mu_0 k_{c2}D_{mn}K_m'(q_2r)]e^{jm\varphi} \tag{18}$$

$$H_r^2(r,\varphi) = -\frac{1}{k_{c2}^2}\sum_{m=0}^{\infty}\sum_{n=1}^{\infty}[\frac{-\omega\varepsilon_2 m}{r}C_{mn}K_m(k_{c2}r) - j\beta k_{c2}D_{mn}K_m'(k_{c2}r)]e^{jm\varphi} \tag{19}$$

$$H_\varphi^2(r,\varphi) = -\frac{1}{k_{c2}^2}\sum_{m=0}^{\infty}\sum_{n=1}^{\infty}[-j\omega\varepsilon_2 k_{c2}C_{mn}K_m'(k_{c2}r) + \frac{\beta m}{r}D_{mn}K_m(k_{c2}r)]e^{jm\varphi} \tag{20}$$

According to the external field equations (17)–(20), we note that the argument $k_{c2}r$ of the modified Bessel function must be real in order to satisfy the radiation condition, thus, $k_{c2} \geq 0$. On the outside of CDRA ($r > a$), the mode is no longer bound to the CDRA. Therefore, the cutoff frequency tends to zero.

Here, we discuss the waveguide modes of a CDRA. Inside a cylindrical dielectric waveguide, the modes can be divided into three types to identify the field variations along the φ, r, and z directions, respectively. These field modes are: transverse electric mode $TE_{mn\delta}$, transverse magnetic mode $TM_{mn\delta}$, and hybrid modes $HE_{mn\delta}$ $(m, n \geq 1)$ and $EH_{mn\delta}$ $(m, n \geq 1)$ [12], [13]. The first index m denotes the order of field variation in the azimuthal plane, the second index n denotes the order of field variation along the radial direction, and the third index $\delta(0 < \delta < 1)$ denotes the order of field variation along the z-direction. In the *TE* mode, $E_z = 0$ along the propagation direction z; in the *TM* mode, $H_z = 0$ along the propagation direction z; and in the hybrid mode, $E_z \neq 0$ and $H_z \neq 0$ along the propagation direction z.

As we can see, the $TE_{0n\delta}$ and $TM_{0n\delta}$ modes have no azimuthal variations for $m = 0$ in their expressions, other modes like $TE_{mn\delta}$ $(m \geq 1)$, $TM_{mn\delta}$ $(m \geq 1)$ and hybrid modes have an azimuth dependency of $e^{jm\varphi}$, which is the general characteristic of OAM.

III. FULLWAVE SIMULATION AND DISCUSSION

In section II we introduced the theoretical analysis to show the OAM features of a CDRA under a certain boundary condition, by using the separation of variables. In this section, an actual CDRA model is adopted to verify the theoretical results by a full wave simulation. The configuration of the cylindrical dielectric resonator antenna (CDRA) is shown in Fig.2. The CDRA with diameter D and length h is placed on the upper side of a substrate, and a metallic ground plane is placed on the lower side of the substrate. The permittivities of the CDRA and the substrate are ε_{CDRA} and ε_{sub}, respectively.

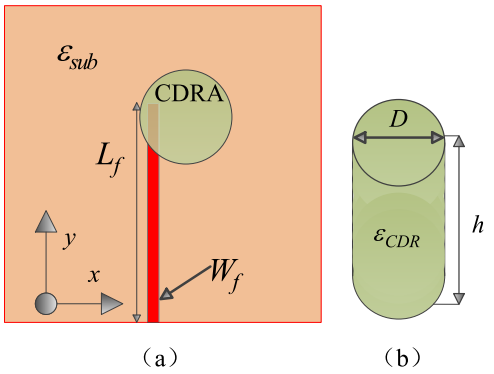

FIGURE 2. A CDRA placed on a substrate, and fed by a microstrip off-center fed line. (a) Top view of CDRA. (b) Geometry of CDR

In order to investigate the OAM features of the CDRA, we made a full wave simulation based on the configuration in Fig.2. The microwave simulation software CST Studio Suite was used for the simulation. As can be seen from the theoretical derivation formulas, under certain conditions with proper size and permittivity and appropriately chosen excitation, the CDRA can radiate OAM waves in some of the electromagnetic modes. Different excitation methods can cause different field mode distributions inside the CDRA, a number of excitation methods have been proposed in the article [16]. As shown in Fig.2, the CDRA is printed on a Rogers substrate with a relative permittivity of $\varepsilon_{sub} = 3.48$, a loss tangent of 0.002, and a substrate thickness of 1.6 mm. The red color in the Fig.2 represents the metal feeding line. The dimension of the substrate is $50 \times 50\ mm^2$. The final parameters of the CDRA in this simulation are $D = 12\ mm$, $h = 10\ mm$, $L_f = 30\ mm$, $W_f = 2\ mm$, $\varepsilon_{CDRA} = 10$. The simulation environment is in free space.

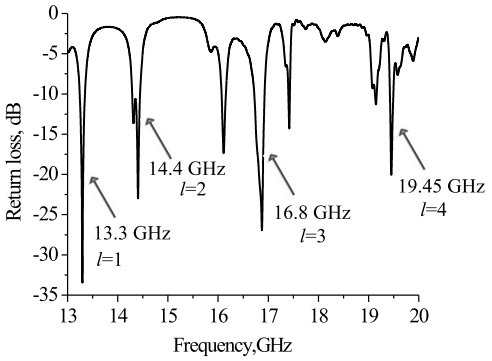

FIGURE 3. Simulated return loss of proposed CDRA.

Fig.3 shows the return loss of the proposed CDRA. As can be seen, the CDRA is a multimode resonant antenna and OAM waves are generated at some of these resonant frequencies. There are eight resonant points across the frequencies between 13 and 20 GHz, four of these resonant frequencies are generated OAM waves with topology charge number $l = 1$ at 13.3 GHz, $l = 2$ at 14.4 GHz, $l = 3$ at 16.8 GHz, $l = 4$ at 19.45 GHz. As can be seen, the largest l is at the highest OAM resonant frequency. This further indicates that higher order OAM will be generated at higher resonant electromagnetic modes.

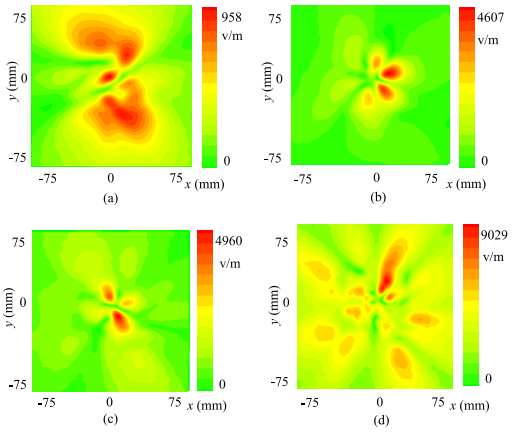

FIGURE 4. Simulated electric field density with different OAM mode numbers. (a) $l = 1$, (b) $l = 2$, (c) $l = 3$, (d) $l = 4$.

Fig.4 and Fig.5 show the simulated amplitude and phase of the radiation electric field in upper side of CDRA, respectively. The observation window is a square area with a dimension of 150 $mm \times 150$ mm. The electrical field intensity observation distance is 20 mm above the upper surface of CDRA. The center of the vortex is exactly aligned with the $+z$ direction, where the electrical field intensity is nearly zero. The rotational phase front of OAM radio beams are obtained from the electric field phase patterns. Fig.5 (a), (b), (c) and (d) show the spiral phase front variations of 1, 2, 3, 4 along the azimuthal plane, respectively. Calculating the numbers of periodic phase variations along the azimuthal direction, clearly demonstrates that the CDRA radiates four OAM radio beams with topological charge number $l = 1, 2, 3, 4$ in $+z$ direction.

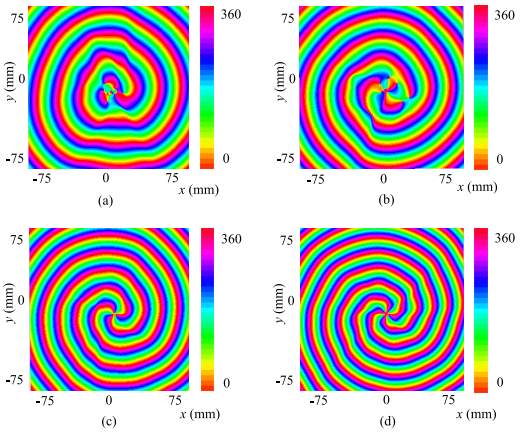

FIGURE 5. Simulated electric field phase with different OAM mode numbers. (a) $l = 1$, (b) $l = 2$, (c) $l = 3$, (d) $l = 4$.

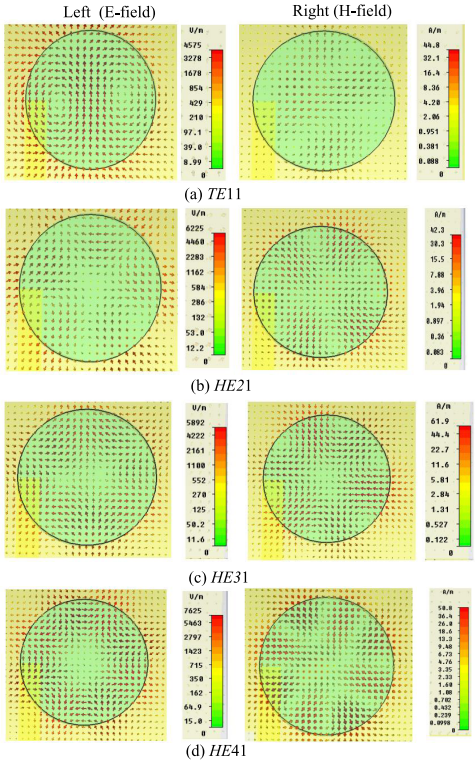

FIGURE 6. Field distributions of proposed CDRA. (a) 13.3 GHz, (b) 14.4 GHz, (c) 16.8 GHz, (d) 19.45 GHz.

Observation confirms the theoretical derivations that a single CDRA can generate multiple OAM modes under certain conditions. Furthermore, as the resonance frequency increases, so does the number of OAM orders.

In order to verify the relationship between electromagnetic modes and OAM modes, Fig.6 shows the transverse view of E-fields and H-fields simultaneously. Here, we don't consider the field variations in $+z$ direction. The observation window is located in the middle of the CDRA ($h = 5$ mm). The left (right) column denotes the E-fields (H-fields) at frequencies 13.3 GHz, 14.4 GHz, 16.8 GHz, 19.45 GHz, respectively. As can be seen from the field patterns:

- TE_{11} is excited at 13.3 GHz to generate the OAM wave with the corresponding topology charge number $l = 1$
- HE_{21} is excited at 14.4 GHz to generate the OAM wave with the corresponding topology charge number $l = 2$
- HE_{31} is excited at 16.8 GHz to generate the OAM wave with the corresponding topology charge number $l = 3$
- HE_{41} is excited at 19.45 GHz to generate the OAM wave with the corresponding topology charge number $l = 4$

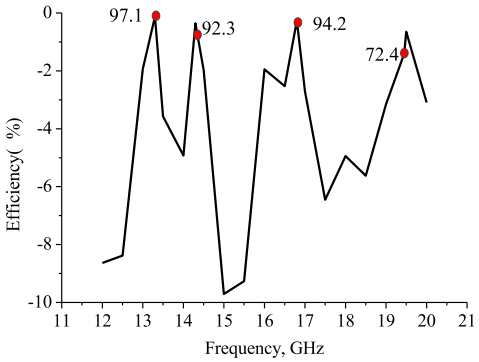

FIGURE 7. Simulated total efficiency of proposed CDRA.

Fig.7 shows the simulated total antenna efficiency of the proposed CDRA. Antenna efficiency is defined as the ratio of the radiation energy to the total energy of feeding. As can be seen from Fig.7, the efficiencies obtained from the four OAM resonant frequencies is high. Specifically, the efficiencies are 97.1% at 13.3 GHz, 92.3% at 14.4 GHz, 94.2% at 16.8 GHz, 72.4% at 19.45 GHz. These results indicate that the CDRA has a maximum radiation efficiency of 97.1% at 13.3 GHz, and a minimum radiation efficiency of 72.4% at 19.45 GHz.

IV. CONCLUSION

In this paper we firstly studied the transmission characteristics of a solid cylindrical dielectric resonator antenna (CDRA) in a cylindrical coordinate system. Secondly, a full-wave simulation on an actual size CDRA was implemented to verify the theoretical results. From the results of the simulations, we conclude that: a) CDRA is an highly efficient and multimode resonant device, which is a promising method to overcome the narrow band and multiband issues existing in the design of current OAM devices; b) only $TE_{mn\delta}$ ($m \geq 1$), $TM_{mn\delta}$ ($m \geq 1$)and hybrid modes can generate OAM waves, the higher order electromagnetic mode is capable of generating higher order OAM wave.

REFERENCES

[1] H. Zhou, J. Dong, S. Yan, Y. Zhou, and X. Zhang, "Generation of terahertz vortices using metasurface with circular slits," *IEEE Photon. J.*, vol. 6, no. 6, Dec. 2014, Art. no. 5900107.
[2] F. E. Mahmouli and S. D. Walker, "4-Gbps uncompressed video transmission over a 60-GHz orbital angular momentum wireless channel," *IEEE Wireless Commun. Lett.*, vol. 2, no. 2, pp. 223–226, Apr. 2013.
[3] Y. Weng, T. Wang, and Z. Pan, "Biomedical photoacoustic imaging sensor based on orbital angular momentum multiplexing," in *Proc. Photon. North*, Jun. 2015, p. 1.
[4] T. Yuan, H. Wang, Y. Qin, and Y. Cheng, "Electromagnetic vortex imaging using uniform concentric circular arrays," *IEEE Antennas Wireless Propag. Lett.*, vol. 15, pp. 1024–1027, 2016.
[5] Matteo Oldoni *et al.*, "Space-division demultiplexing in orbital-angular-momentum-based MIMO radio systems," *IEEE Trans. Antennas Propag.*, vol. 63, no. 10, pp. 4582–4587, Oct. 2015.
[6] F. Tamburini, E. Mari, B. Thide, C. Barbieri, and F. Romannato, "Experimental verification of photon angular momentum and vorticity with radio techniques," *Appl. Phys. Lett*, vol. 8, no. 3, pp. 260–267, 2011.
[7] M. Barbuto, F. Trotta, F. Bilotti, and A. Toscano, "Circular polarized patch antenna generating orbital angular momentum," *Prog. Electromagn. Res.*, vol. 148, pp. 23–40, 2014.
[8] X. Hui *et al.*, "Ultralow reflectivity spiral phase plate for generation of millimeter-wave OAM beam," *IEEE Antennas Wireless Propag. Lett.*, vol. 14, pp. 966–969, 2015.
[9] Q. Bai, A. Tennant, and B. Allen, "Experimental circular phased array for generating OAM radio beams," *Electron. Lett*, vol. 50, no. 20, pp. 1414–1415, Sep. 2014.
[10] H. W. Wu *et al.*, "Cavity modes with optical orbital angular momentum in a metamaterial ring based on transformation optics," *Opt. Exp.*, vol. 23, no. 25, pp. 32087–32097, 2015.
[11] X. Bai *et al.*, "Design of a horn lens antenna for OAM generation," *IEEE Antennas Wireless Propag. Lett.*, vol. 14, pp. 2081–2082, 2015.
[12] C. Yeh and F. I. Shimabukuro, *The Essence of Dielectric Waveguide*. Springer: New York, GER, 2008.
[13] R. K. Mongia and P. Bhartia, "Dielectric resonator antennas—A review and general design relations for resonant frequency and bandwidth," *Int. J. Microw. Millimeter-Wave Comput.-Aided Eng.*, vol. 4, no. 3, pp. 230–247, Jul. 1994.
[14] G. N. Malheiros-Silveira, G. S. Wiederhecker, and H. E. Hernández-Figueroa, "Dielectric resonator antenna for applications in nanophotonics," *Opt. Exp.*, vol. 21, no. 1, pp. 1234–1239, 2013.
[15] L. Zou *et al.*, "Efficiency and scalability of dielectric resonator antennas at optical frequencies," *IEEE Photon. J.*, vol. 6, no. 4, Aug. 2014, Art. no. 4600110.
[16] K. M. Luk, and K. W. Leung, *Dielectric Resonator Antennas*. England, Research Studies Press ltd, 2003.
[17] Y. Pan *et al.*, "Generation of orbital angular momentum radio waves based on dielectric resonator antenna," *IEEE Antennas Wireless Propag. Lett.*, doi: 10.1109/LAWP.2016.2578958, 2016.

JIAJUN LIANG received the B.E. degree in electronic science and technique from the Guilin University of Electronic Technology, Guilin, China, in 2012, and the M.E. degree in radio physics from the University of Electronic Science and Technology of China, Chengdu, China, in 2015. He is currently pursuing the Ph.D. degree in information and communication engineering with Shenzhen University, Shenzhen, China. His current research interests include RF OAM antennas, filtering antennas, and duplex antenna.

SHENGLI ZHANG received the B.E. degree in electronic engineering and the M.E. degree in communication and information engineering from the University of Science and Technology of China (USTC), Hefei, China, in 2002 and 2005, respectively, and the Ph.D. degree from the Department of Information Engineering, The Chinese University of Hong Kong (CUHK), in 2008. From 2002 to 2005, he was with the Personal Communication Network and Spread Spectrum Laboratory, USTC, as a Research Engineer involved in several National 863 Research Projects, including the Beyond-3 Generation of Mobile System in China (FUTURE Plan). From 2002 to 2005, he was also a Research Engineer of the UTStarcom Wireless Soft Research Center, Hefei, China, involved in the research and implementation of WCDMA communication systems. Since 2008, he was a Research Associate with CUHK. He is currently an Associate Professor with Communication Engineering Department, Shenzhen University, China. His current research interests include wireless networks, wireless communication, physical layer network coding, and cooperative wireless networks.